Scanning Microscopy

Volume 6 | Number 1 Article 11

1-25-1992

Nuclear Microprobe Application in Semiconductor Process Developments

Mikio Takai
Osaka University

Scanning Microscopy, Vol. 6, No. 1, 1992 (Pages 147-156) 0891-7035/92$5.00+.00
Scanning Microscopy International, Chicago (AMF O'Hare), IL 60666 USA

NUCLEAR MICROPROBE APPLICATION IN SEMICONDUCTOR PROCESS DEVELOPMENTS

Mikio Takai

Faculty of Engineering Science and Research Center for Extreme Materials,
Osaka University, Toyonaka, Osaka 560, Japan

(Received for publication May 6, 1991, and in revised form January 25, 1992)

Abstract

Scanning nuclear microprobes using Rutherford backscattering (RBS) with light ions have been applied to semiconductor process steps, in which minimum feature sizes of several microns down to submicron and multi-layered structures were used. Two or three dimensional RBS mapping of processed semiconductor layers such as multi-layered wiring, semiconductor-on-insulator (SOI), focused ion implanted layers, and laser processed layers, has clearly revealed process failures and inhomogeneity in buried layers without layer removal processes. Radiation damage due to the probe beams was found to be induced by high probe doses at and above $10^{17}/cm^2$, in which the degradation of crystallinity by probe beams differs between Si and GaAs.

Key Words: nuclear microprobe, Rutherford backscattering (RBS), RBS tomography, RBS mapping, channeling contrast mapping, focused ion beam, three dimensional analysis, semiconductor, wiring, maskless process.

Address for correspondence:
Mikio Takai, Faculty of Engineering Science,
Osaka University, Toyonaka, Osaka 560, Japan
Phone: +81-6-844-1151
Fax: +81-6-857-7664

Introduction

Ion beam analysis with Rutherford backscattering (RBS) and channeling has been successfully used for device process development in the early stage of application of ion implantation in semiconductors [30-33]. Such studies have substantially enhanced today's CMOS (Complementary Metal Oxide Semiconductor) technology for IC's. Following this early time, the feature size of IC's has shrunk from several microns down to submicron dimensions, where scanning microscopy using electron beams such as SEM and Auger has played an important role for developing and inspecting IC structures with small minimum-feature-size.

Such electron beam probes, however, can detect only the top surface of device structures. Such techniques also suffer charge-up effects for insulating layers on device structures. Furthermore, three dimensional structures such as multi-layered wiring or semiconductor-on-insulator (SOI) structures [34] require not only lateral but also in-depth information without using layer removal processes such as sputtering. Future maskless semiconductor processes such as maskless doping, etching and deposition using focused ion or laser beams must be locally analyzed to optimize their process steps.

Ion scanning microprobes with RBS, on the other hand, can provide information on the atomic composition and distribution of both matrix materials and impurity atoms beneath insulating layers substantially without suffering charge-up effects [5,27,43]. Local crystallinity in a semiconductor substrate can also be analyzed when RBS and channeling are combined with ion microprobes [26,28].

In this study, nuclear microprobes with light ions have been applied to semiconductor process steps such as multi-layered wiring, SOI, maskless

ion implantation, and laser chemical vapor deposition (CVD). Problems arising from the nuclear microprobe measurement such as radiation damage due to probe beams are clarified.

Experimental

Two beam lines were used for nuclear microprobe analysis with proton and helium ions. One was connected with a 2 MeV Van de Graaff [9,14-16,22,35,36,39] and the other with a 500 keV Disktron (rotating-disk type accelerator) connected also with a UHV (ultra high vacuum) chamber and toroidal energy analyzer [1-3, 10-13,38,40]. The beam optics for the microprobes in the two beam lines consisted of variable object slits and a quadrupole doublet with a minimum beam spot diameter of less than 1 micron at FWHM (full width at half maximum) and a current of 100 pA [9-12,35,38,41]. The beam current was reduced to suppress radiation damage during measurement as mentioned elsewhere [13,42]. RBS and channeling were mostly used with microprobes because analysis of semiconductor process steps required good lateral and in-depth resolutions [9,35,36]. Figure 1 shows the schematic of RBS mapping [9,35] and tomography (or cross-sectional mapping) [19,21] used in this study. A microprobe is scanned over the sample. The RBS spectrum for each of the microprobe positions is stored in memory. RBS mapping at a required depth (or energy) can be obtained by selecting yields in the appropriate channels of micro RBS spectra in each of the microprobe positions or pixels (as in Fig. 1). The cross-sectional information (RBS tomography) can be obtained by selecting a set of micro RBS spectra in a required line [19,21].

Results and Discussion

Multi-layered wiring isolated with insulating layers. One of the most important problems for recent IC structures is multi-layered structures for wiring [9,14,15,19,23,37], which consist of metal lines isolated with insulating layers such as silicon dioxide or nitride. Figure 2 shows the schematic of a test structure representing multi-layered wiring (a), a corresponding RBS spectrum (b), and RBS mapping images (c) for each of 4 gold stripe layers. The test structure has four layers of gold (Au) stripe patterns offset by 45 degrees with respect to each other to correctly identify each layer by RBS mapping images. The RBS spectrum obtained with a defocused beam shows three major

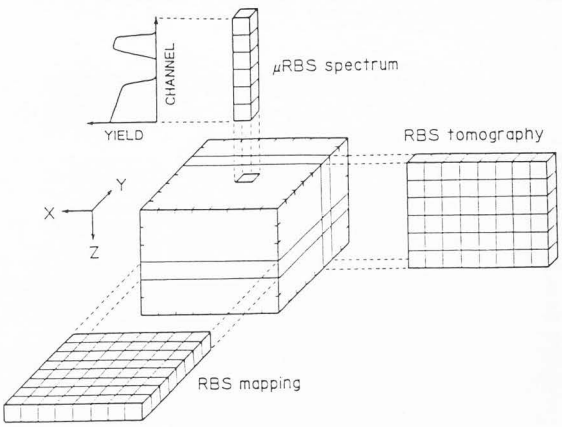

Figure 1. Schematic of RBS mapping and tomography with microbeams

peaks due to gold stripe patterns in each of the layers. The 2nd and the 3rd Au signals overlap because the thickness of the insulating layer between two Au layers is thinner than that of the 1st and the 3rd insulating layers. The RBS mapping images corresponding to the test structure can be obtained by setting four energy windows for each of the RBS peaks as in Fig. 2b. Although the image of the 1st layer is clearly obtained in Fig. 2c, the influence of the surface Au layer causes a difference in beam paths of incident and scattered particles, giving rise to the broadening of the spectrum width, which broadens of the patterns in the images of the lower layers. It should be noted that four-layered wiring images can be nondestructively obtained within 20 to 30 min with a probe dose of 3 - 8 x $10^{15}/cm^2$.

Figure 3 shows the cross-sectional view of a similar structure shown in Fig.2 and corresponding RBS tomography for two different planes: one is a scan along the gold stripe (a) and the other along the silicon dioxide layer (b). The vertical axis stands for the channel number of the micro RBS spectrum (i.e., energies of scattered particles), corresponding to a depth scale. The horizontal axis stands for positions of the microprobe. Therefore, the mapping images show the tomograph of the gold stripe patterns. Because of the difference in paths of the microprobe beam, the location of images of the second to fourth layers in Fig.3b-(b) shifts by about 10 channels to higher energy compared to the Fig.3b-(a). Therefore it is necessary to take account of the influence of the upper layer for correcting such deformation of the images. However, the cross-sectional structure of multi-layered wiring can be clearly imaged without cleaving the sample.

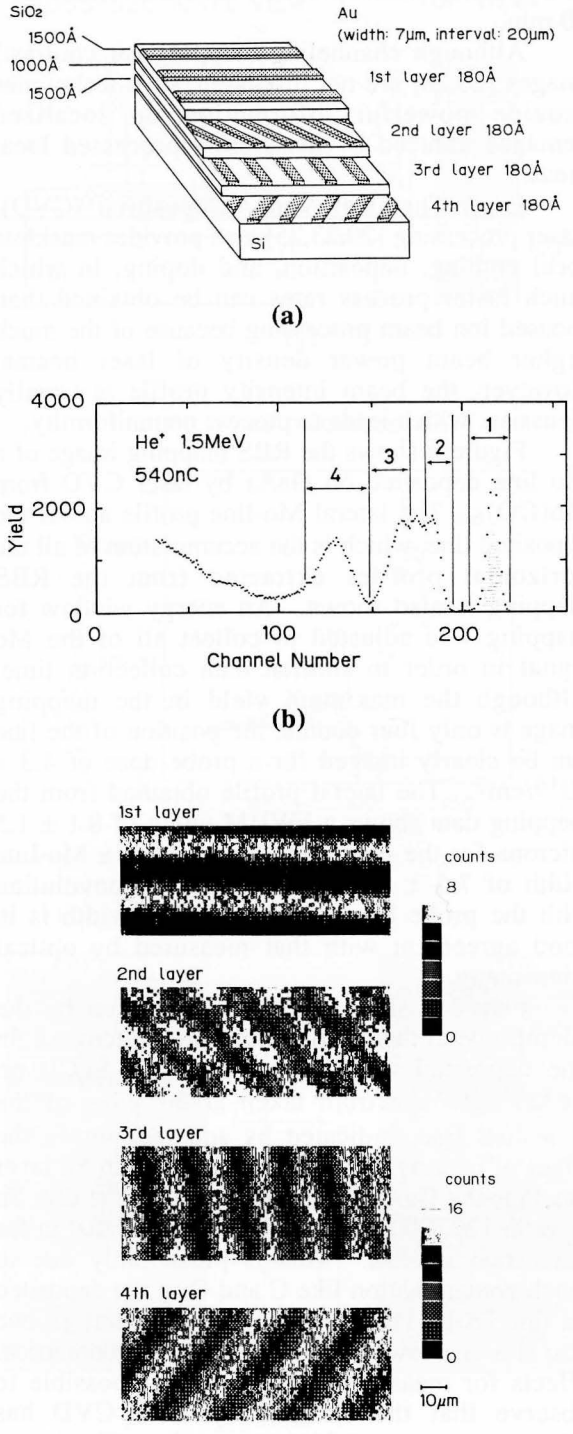

Figure 2. Schematic of a test structure for multi-layered wiring insulated with silicon dioxide layers (a), corresponding RBS spectrum with a defocused probe beam (b) and two dimensional mapping with a focused probe beam(c)

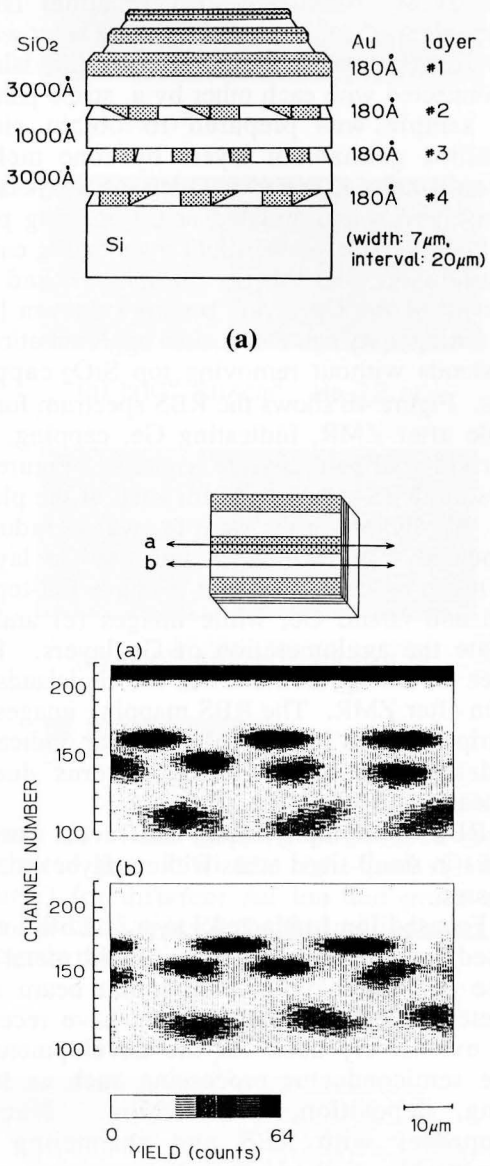

Figure 3. Schematic of a test structure for multi-layered wiring, showing a cross-sectional view (a), and corresponding RBS tomography (b)

Semiconductor-on-insulator (SOI) Structure. Figure 4a shows the top and cross-sectional views of a semiconductor-on-insulator structure [21,23,24,34] consisting of germanium island patterns on a silicon dioxide insulating layer with a silicon dioxide capping layer. Germanium islands are connected with each other by a stripe pattern. This sample was prepared to obtain single crystalline germanium layers by zone melting recrystallization (ZMR), in which the temperature of Ge layers was regulated at the melting point (937 ^{o}C)[34]. However, slight overheating causes the agglomeration of Ge in islands and the thickness of the Ge layers becomes uneven [34]. RBS tomography can detect such agglomeration of Ge islands without removing top SiO_2 capping layers. Figure 4b shows the RBS spectrum for the sample after ZMR, indicating Ge, capping, and underlying silicon dioxide signals. Figure 4c shows the RBS tomographs for each of the planes (a - h), where the sample was gradually overheated. Black images indicate Ge layers. RBS mapping images (a) and (b) have flat-topped stripe and island Ge, while images (e) and (f) indicate the agglomeration of Ge layers. RBS images (c) and (g) indicate that the Ge islands are broken after ZMR. The RBS mapping images for Ge stripe patterns (d) and (h) disappear, indicating the destruction of the stripe patterns due to overheating.

RBS tomography, thus, can reveal process failures in small sized areas without layer removal processes.

Focused Ion Implanted Layer. Low energy focused ion implanters with a liquid metal ion source [17,18], having a minimum beam spot diameter of less than 0.1 micron, have recently been extensively used for the development of future semiconductor processing such as local doping, deposition, and etching. Nuclear microprobes with RBS and channeling are indispensable methods for characterizing such locally processed areas.

Figure 5 shows the He-RBS mapping with an energy window set on Au for Si samples locally implanted with Au ions at 100 keV to a dose of 1 - 6 x $10^{16}/cm^2$. Since the implanted Au lines cannot be detected by SEM, a gold electrode pad is used to easily locate probe beams for this measurement. Bright patterns on the left-hand side of the images are the gold pad patterns. Line shaped dot patterns to the right are gold implanted lines of different implant and analysis doses. Although the yield for the gold implanted lines is a few counts, it is possible to detect locally implanted Au lines in Si by nuclear microprobes with RBS within 60 - 90 min.

Although channeling mapping (or contrast) images [26,28] are not discussed, such techniques provide powerful information on localized damages induced by masklessly processed local areas.

Laser Chemical Vapor Deposition (CVD). Laser processing [20,23,25] also provides maskless local etching, deposition, and doping, in which much faster process rates can be obtained than focused ion beam processing because of the much higher beam power density of laser beams. However, the beam intensity profile is usually Gaussian, which leads to process nonuniformity.

Figure 6 shows the RBS mapping image of a Mo line deposited on GaAs by laser CVD from $Mo(CO)_6$. The lateral Mo-line profile across the deposited line, which is the accumulation of all the horizontal profiles extracted from the RBS mapping is also shown. An energy window for mapping was adjusted to collect all of the Mo signal in order to shorten data collection time. Although the maximum yield in the mapping image is only four counts, the position of the line can be clearly imaged for a probe dose of 4.3 x $10^{16}/cm^2$. The lateral profile obtained from the mapping data shows a FWHM width of 8.1 $\pm$ 1.5 microns for the line. This converts to a Mo-line width of 7.5 $\pm$ 1.6 microns after deconvolution with the probe beam diameter. This width is in good agreement with that measured by optical microscopy.

Figure 7 shows RBS spectra taken by the microprobe at three different positions across a Sn line deposited with laser CVD from $SnCl_4$ on GaAs. The spectrum taken at the edge of the deposited line, indicated by squares, shows the edges of underlying GaAs, where the thin Sn layer overlaps the GaAs layer. The yield of the thin Sn layer in 120 -200 channels is lower than that in the other two spectra. This is presumably due to much contamination like C and O in the deposited Sn line [20]. The spectrum of the central groove also shows a low yield because of the geometrical effects for measurement. Thus it is possible to observe that the Sn line by laser CVD has inhomogeneous stoichiometry and profile due to the intensity profile of the laser beam.

Radiation Damage due to Probe Beam. Although the nuclear microprobe with RBS is a powerful tool for characterizing semiconductor process steps, it is necessary to irradiate samples with a high probe dose [13,42] because of the low yield from micron sized areas. Heavy ion

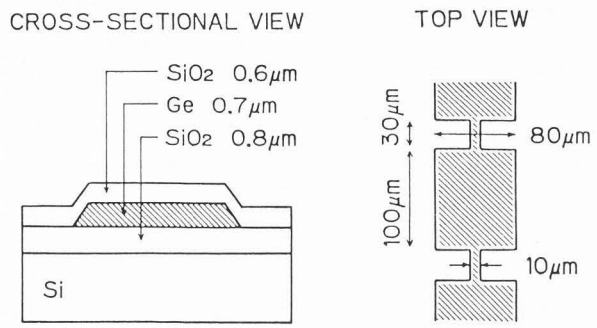

(a)

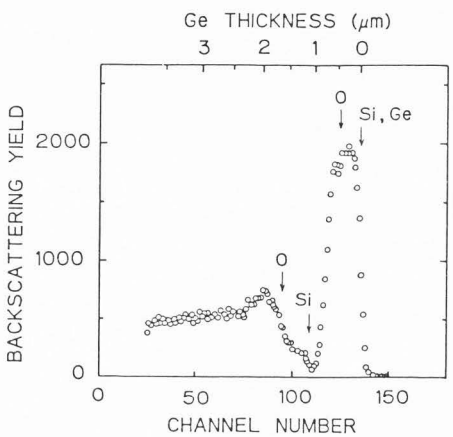

(b)

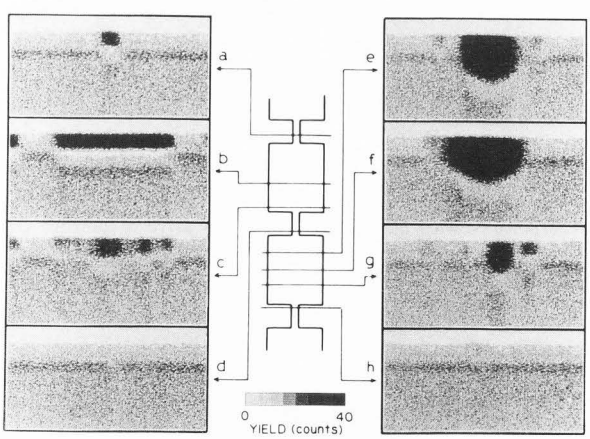

(c)

Figure 4. Schematic of germanium on insulator structure capped with silicon dioxide layer (a), corresponding RBS spectrum with defocused 1.8 MeV H_2 ion probe beam (b), and RBS tomography for each of the positions with focused probe beams (c).

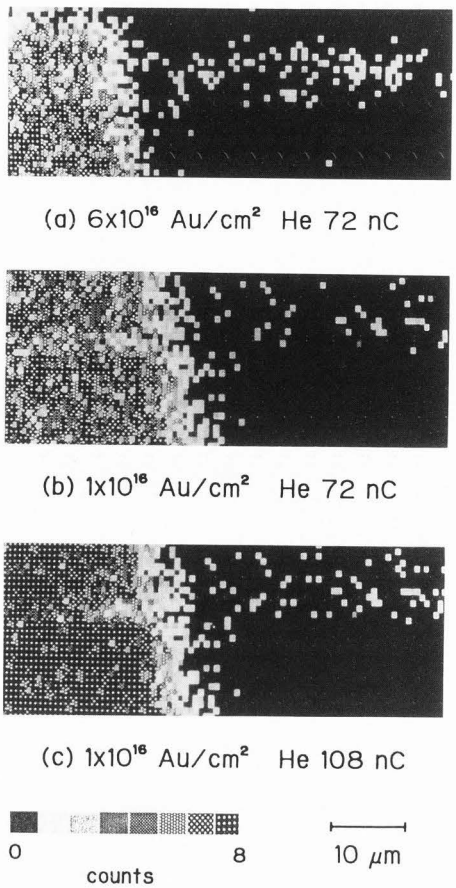

Figure 5. RBS mapping of focused Au ion-implanted lines in Si (the right-hand side of the figures) for different Au ion and probe doses. The left-hand side of the figures indicates gold-electrode pads.

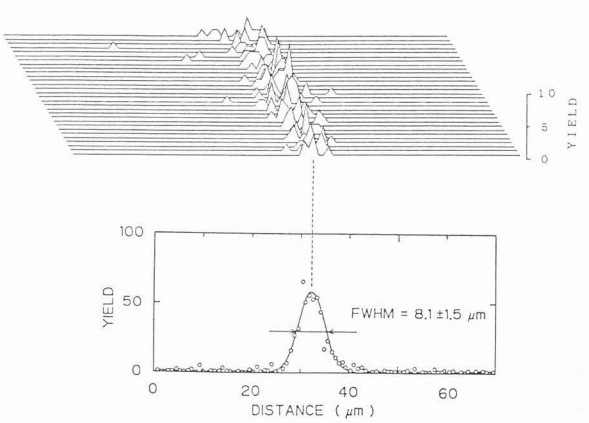

Figure 6. RBS mapping image for laser-CVD Mo line and integrated distribution profile across the line

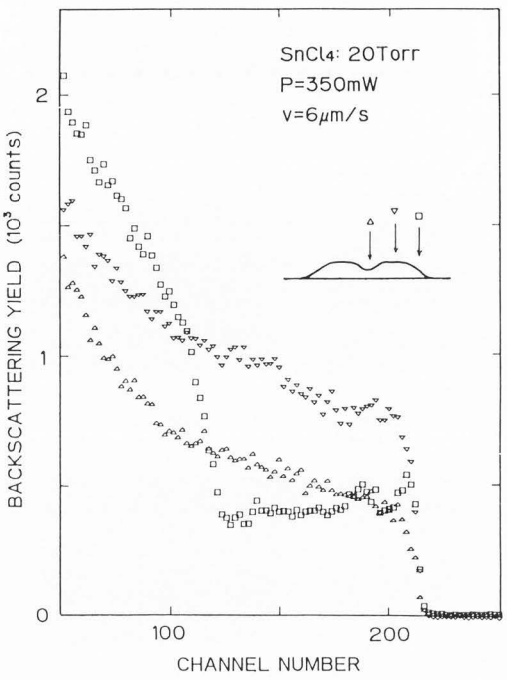

Figure 7. Localized RBS spectra for each of the positions across the laser-CVD SnO line. The SnO line was deposited in 20 Torr $SnCl_4$ atmosphere with a laser power of 350 mW at a beam scanning speed of 6 micron/s.

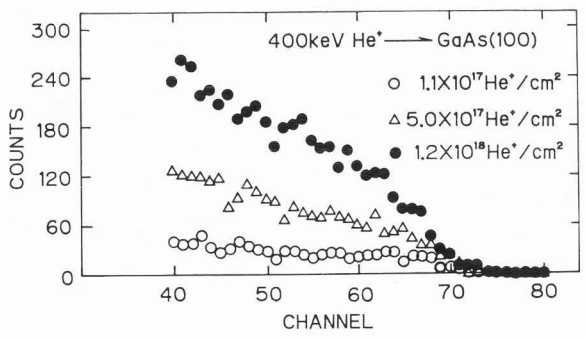

Figure 8. Aligned RBS spectra for GaAs samples irradiated with three different doses of probe beams. The probe dose for RBS spectrum was 5 x $10^{15}/cm^2$.

microprobes, indeed, have much higher scattering cross-section for RBS and good mass resolution [6,7,8]. However, radiation damage by probe beams is much more severe. Therefore, radiation damage due to probe beams is one of the important problems when this technique is applied to single crystalline semiconductors.

Figure 8 shows RBS spectra at various microprobe doses under a channeling condition for 400 keV helium on (100) GaAs. The yield for the channeling spectrum drastically increases with the increase in probe beam dose at and above 5 x $10^{17}/cm^2$, suggesting the degradation of crystallinity of GaAs. This result indicates that the probe dose must be kept at and below 1 x $10^{17}/cm^2$ in this case.

Figure 9 shows the minimum scattering yield taken at the surface region of channeled spectra normalized to random yield for GaAs and Si as a function of probe helium dose. The yield gradually increases with increase in probe dose above $10^{17}/cm^2$ and depends on the probe current density for GaAs, while for Si the yield abruptly increases at $10^{18}/cm^2$ and the behavior does not depend on the probe current density. A similar probe-current density-dependence on damage rate in GaAs was observed for high energy microprobes with 1 - 2 MeV helium ions [4,29]. This difference in the degradation of crystallinity between GaAs and Si is considered as follows: vacancies created by probe beams in GaAs are not easily annealed at room temperature because GaAs has two atomic sites (Ga-site and As-site) [31,32], while vacancies created in Si are easily annealed at room temperature at a probe dose below $10^{18}/cm^2$. The increase in the normalized yield for Si at a probe dose above $10^{18}/cm^2$ is considered to be due to the swelling of the irradiated area because of a volume change of more than 60 % by helium implantation as discussed elsewhere [13,42]. At higher probe doses than 5 x $10^{18}/cm^2$, ablation occurs in the irradiated Si layer [42].

Thus, the radiation damage due to the probe beam is much more critical for compound semiconductors like GaAs than Si.

Problems other than radiation damage are the minimum probe beam spot diameter when this nuclear microprobe is applied to future semiconductor process steps. The minimum feature size is still shrinking from half a micron to a quarter micron, in which case much smaller beam spot diameters of probe beams will be required. Therefore, a nuclear microprobe with a beam spot diameter of less than 0.05 micron will

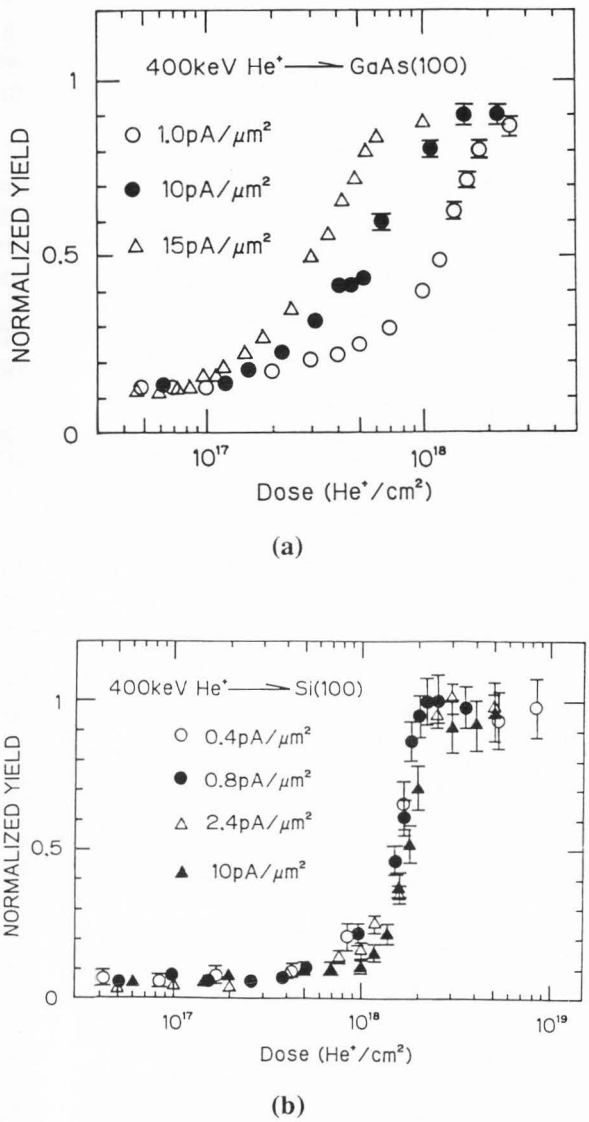

Figure 9. Normalized yield of aligned RBS spectra for GaAs (a) and Si (b) samples as a function of probe dose with different probe current densities

be required for future applications in the semiconductor field. One possible system will be with a high brightness ion source such as a field ion emission source with helium or Li ions combined with a short acceleration column with a high energy-resolution analyzer for RBS. Such a system must be compact enough for the use in a clean room for semiconductor processing. Minimization in probe spot-diameter gives rise to decrease in RBS scattering yield and, hence, large areal mapping becomes difficult. Channeling mapping would not be feasible with future 0.05 micron probebeams because the channeling yield further decreases by more than one order of magnitude.

Conclusions

Nuclear microprobes combined with RBS can successfully be applied in semiconductor process developments such as multi-layered structures like SOI and multi-layered wiring, maskless implantation, and maskless laser induced deposition. However, radiation damage due to probe beams must be taken into consideration when good statistics for measurement are required. Further minimization in the probe beam diameter will be expected for application of this technique to future semiconductor process steps, in which minimum feature sizes of a quarter micron will be utilized. In such a case, channeling mapping will work only in small areas such as a few microns squares.

Acknowledgement

This work was partly supported by the System of Joint Research with Industry (Kobe Steel, Ltd., ULVAC Japan, Ltd., and the Ministry of Education, Science and Culture). The author is indebted to his colleagues, S. Namba, A. Kinomura, and K. Hirai of Osaka University and to M. Satou, A. Chayahara, and Y. Horino of Government Industrial Research Institute Osaka.

References

1. Agawa Y, Uchiyama T, Hoshino A, Tsuboi H, Fukui R, Takagi K, Yamakawa H, Matsuo T, Takai M, Namba S (1990) 500 keV ion beam accelerator for microbeam formation. Nucl. Instr. and Methods B45: 540 - 542.

2. Agawa Y, Takai M, Ishibashi K, Hirai K, Namba S (1990) Influence of current ripple on secondary electron and RBS mapping images. Japan. J. Appl. Phys.29: L1011 - L1014.

3. Agawa Y, Takai M, Namba S, Uchiyama T, Fukui R, Yamakawa H (1991) A 500 keV ion accelerator with two types of ion source. Nucl. Instr. and Methods B55: 502 - 505.

4. Brown RA, McCallum JC, Williams JS (1991) 2 MeV He microbeam damage in Si and

GaAs. Nucl. Instr. and Methods B54:197 - 203.

5. Grime GW, Watt F (1988) Nuclear Microprobe Technology and Applications. North-Holland, Amsterdam, 227 - 506.

6. Horino Y, Chayahara A, Kiuchi M, Fujii K, Satou M, Takai M (1990) Microbeam line of MeV heavy ions for materials modification and in-situ analysis. Japan. J. Appl. Phys. 29: 2680 - 2683.

7. Horino Y, Chayahara A, Kiuchi M, Fujii K, Satou M, Takai M (1991) A focused MeV heavy ion beam line for materials modification and micro analysis. Nucl. Instr. and Methods B59/60: 139 - 144.

8. Horino Y, Chayahara A, Satou M, Takai M (1991) 3-dimensional microanalysis using focused MeV oxygen ion beam. Nucl. Instr. and Methods B (in press)

9. Inoue K, Takai M, Matsunaga K, Izumi M, Gamo K, Namba S, Satou M (1988) Microbeam line with 1.5 MeV helium ions and protons at Osaka. Nucl. Instr. and Methods B30: 580 - 591.

10. Inoue K, Ishibashi K, Kawata Y, Suzuki N, Takai M, Namba S (1989) 0.5 MeV submicron ion probe system for RBS/PIXE. In: Processing and Characterization of Materials Using Ion Beam, Rehn LE, Greene JE, Smidt FA (eds), Materials Research Society, Pittsburgh, 381 - 386

11. Inoue K, Takai M, Ishibashi K, Kawata Y, Namba S (1989) Magnetic analysis of quadrupole lens for MeV ion microprobe. Japan. J. Appl. Phys. 28: L1307 - L1309.

12. Inoue K, Takai M, Ishibashi K, Kawata Y, Suzuki N, Namba S (1990) Focused 0.5 MeV ion beam line with low aberration quadrupole magnets. In: Beam-solid Interactions: Physical Phenomena, Borgesen P, Knapp JA, Zuhr RA (eds), Materials Research Society, Pittsburgh, 329 - 334.

13. Inoue K, Takai M, Ishibashi K, Hirai K, Kawata Y, Namba S (1991) Damage induced during channeling measurement with a nuclear microprobe. Nucl. Instr. and Methods B54: 231 - 233.

14. Kinomura A, Matsunaga K, Inoue K, Izumi M, Takai M, Gamo K, Namba S, Kiuchi M, Satou M (1987) Micro RBS analysis by focused 1.5 MeV ion beam. In: Proc. of the 19th Conf. on Solid State Devices and Materials, Tokyo, 467 - 470.

15. Kinomura A, Takai M, Inoue K, Matsunaga K, Izumi M, Matsuo T, Gamo K, Namba S, Satou M (1988) Microprobe using focused 1.5 MeV helium ion and proton beam. Nucl. Instr. and Methods B33: 862 - 866.

16. Kinomura A, Takai M, Matsuo T, Kiuchi M, Fujii K, Satou M, Namba S (1988) Optimization in spot sizes of focused MeV ion beam by precise adjustment of lens-current excitations. Japan. J. Appl. Phys. 27: L1346 - L1348.

17. Kinomura A, Takai M, Matsuo T, Ujiie S, Namba S, Satou M, Kiuchi M, Fujii K (1989) RBS analysis of beam-processed micro area by focused MeV ion beam . Nucl. Instr. and Methods B39: 40 - 42.

18. Kinomura A, Takai M, Matsuo T, Namba S, Satou M, Kiuchi M, Fujii K (1989) Micro-RBS analysis of masklessly fabricated structures. In: Processing and Characterization of Materials Using Ion Beam, Rehn LE, Greene JE, Smidt FA (eds), Materials Research Society, Pittsburgh, 743 - 748.

19. Kinomura A, Takai M, Matsuo T, Satou M, Chayahara A, Namba S (1989) Tomography of microstructures by scanning micro-RBS probe. Japan. J. Appl. Phys. 28: L1286 - L1289.

20. Kinomura A, Takai M, Namba S, Satou M, Chayahara A (1990) Characterization of masklessly deposited metal lines by micro-RBS probe. Nucl. Instr. and Methods B45: 536 - 539.

21. Kinomura A, Takai M, Namba S, Satou M, Chayahara A (1990) RBS tomography of SOI structures using MeV ion microprobe. Nucl. Instr. and Methods B45: 523 - 526.

22. Kinomura A, Takai M, Namba S (1989) Quick focus adjustment for quadrupole lens system to form high energy ion microbeam. Japan. J. Appl. Phys. 28: L1644-L1646.

23. Kinomura A, Takai M, Namba S, Satou M, Chayahara A (1989) Inspection of inner layer structures by micro-RBS tomography. In: Proc. of Intern. Meeting on Advanced Processing and Characterization Technologies, Japan Society of Applied Physics, Tokyo, 31-34.

24. Kinomura A, Takai M, Namba S (1991) Image processing for three-dimensional analysis by MeV ion microprobe. Nucl. Instr. and Methods B54:275 - 278.

25. Kinomura A, Takai M, Satou M, Chayahara A, Namba S (1990) Evaluation of compositional change in masklessly deposited lines by micro-RBS analysis. In: Beam-solid Interactions: Physical Phenomena, Borgesen P, Knapp JA, Zuhr RA (eds), Materials Research Society, Pittsburgh, 311 - 316.

26. Kinomura A, Takai M, Hirai K Namba S (1991) Channeling contrast analysis of local defect distributions formed by maskless ion-

implantation. Nucl. Instr. and Methods B55: 866 - 869.

27. Legge GJF, Jamieson DN (1991) Nuclear Microprobe Technology and Applications. North-Holland, Amsterdam, 1 - 446.

28. McCallum JC, Mckenzie CD, Lucas MA, Rossiter KG, Short KT, Williams JS (1983) Channeling contrast microscopy: application to semiconductor structures. Appl. Phys. Lett. 42: 827 - 829

29. Piette M and Bodart F (1991) A study of damage induced in semiconductors and metals during microchanneling measurements. Nucl. Instr. and Methods B54: 204 - 208

30. Ryssel H, Ruge I (1986) Ion Implantation. John Wiley & Sons, Chichester, 316 - 374

31. Takai M, Gamo K, Masuda K, Namba S (1973) Effects of implantation temperature on lattice location of tellurium implanted in gallium arsenide. Japan. J. Appl. Phys. 12: 1926 - 1930.

32. Takai M, Gamo K, Masuda K, Namba S (1975) Lattice site location of cadmium and tellurium implanted in gallium arsenide. Japan. J. Appl. Phys. 14: 1935 - 1941.

33. Takai M, Ishida T, Gamo K, Masuda K, Namba S, Mizobuchi A (1977) Lattice-site locations of tin and antimony implanted in gallium phosphide. Japan. J. Appl. Phys. 16: 1853 - 1858.

34. Takai M, Tanigawa T, Gamo K, Namba S (1983) Single crystalline germanium island on insulator by zone melting recrystallization. Japan. J. Appl. Phys. 22: L624 - L626.

35. Takai M, Matsunaga K, Inoue K, Izumi M, Gamo K, Satou M, Namba S (1987) Microanalysis by focused MeV helium ion beam. Japan. J. Appl. Phys. 26: L550 - L553.

36. Takai M, Kinomura A, Inoue K, Matsunaga K, Izumi M, Gamo K, Satou M, Namba S (1988) Focused MeV beam line for microanalysis at Osaka. Nucl. Instr. and Methods B30: 260 - 264

37. Takai M, Kinomura A, Izumi M, Matsunaga K, Inoue K, Gamo K, Namba S, Kiuchi M, Satou M (1988) Multilayer analysis by focused MeV ion beam. In: Electronic Packaging Materials Science, Jaccodine R, Jackson KA, Sundahl RC (eds), Materials Research Society, Pittsburgh, 51 - 56.

38. Takai M, Matsuo T, Namba S, Inoue K, Kawata Y, Ishibashi K (1989) Microbeam line design for medium to high energy helium ion beams. Nucl. Instr. and Methods B37/38: 260 - 263.

39. Takai M, Kinomura A, Matsuo T, Namba S, Satou M, Kiuchi M, Fujii K (1989) Influence of excitation current deviation of quadrupole magnet on beam spot size for MeV micro beams. Nucl. Instr. and Methods B37/38: 244 - 247

40. Takai M, Matsuo T, Kinomura A, Namba S, Inoue K, Kawata Y, Ishibashi K (1990) Microbeam line for medium energy ion beams. Nucl. Instr. and Methods B45: 553 - 556.

41. Takai M, Agawa Y, Ishibashi K, Hirai K, Namba S (1991) Influence of ion beam fluctuation on secondary electron and RBS mapping images. Nucl. Instr. and Methods B54: 279 - 283.

42. Takai M, Hirai K, Ishibashi K, Kinomura A, Namba S (1991) Evaluation of beam-induced ablation during microbeam irradiation. Nucl. Instr. and Methods B54: 209 - 212.

43. Watt F, Grime W (1987) Principles and Applications of High-Energy Ion Microbeams. Adam Hilger, Bristol, 1 -399.

Discussion with Reviewers

D.N. Jamieson and B.L. Doyle: The tomographic image obtained in this paper is not true cross-section views of the sample because of artifacts that arise from the differing surface energies of the elements in the sample.

Author: An exact tomographic image should be obtained as a function of depth instead of energy as you pointed out. Further reconstruction of RBS spectra is necessary to obtain the exact tomography. In this paper, I only compared the depth distributions of particular regions of the same elements, say Au in SiO_2, so that this technique is still valuable. Reconstruction procedures of RBS tomography will be published elsewhere.

L.H. Allen: Most interconnect metal and isolating layers will be much thicker than 18 and 150 nm used in this paper (assuming samples are planarized). How will this method be used for more realistic metal thicknesses in the 1000 nm range?

Author: A proton microprobe instead of helium ion probes can be used as in the case of Fig. 4 in order to get tomographic images with such a thick metal layer.

N. Cheung: The examples chosen all show non-overlapping signals with those of the substrate elements. A general procedure for deconvolution

signals is not described in the paper.
Author: For clarity, I presented the examples without signal overlapping. RBS mapping techniques described in this paper have limitations which conventional RBS techniques with a beam spot-size of 0.5 mm also have. The procedure for deconvolution is the same with that for conventional RBS cases.

N. Cheung: For the SOI example, optical microscopy or thermal wave mapping can provide similar information on island formation.
Author: RBS mapping can provide unique information of semiconductor layers alone (such as agglomeration under capping layers) without removing the top capping layers.